MATERIALS CHEMISTRY
FRONTIERS

Accepted Manuscript

This article can be cited before page numbers have been issued, to do this please use: C. J. Howard, J. Yan, A. Oladokun, Z. Zheng, B. Jaeger, W. Wang and J. G. Werner, *Mater. Chem. Front.*, 2026, DOI: 10.1039/D6QM00261G.

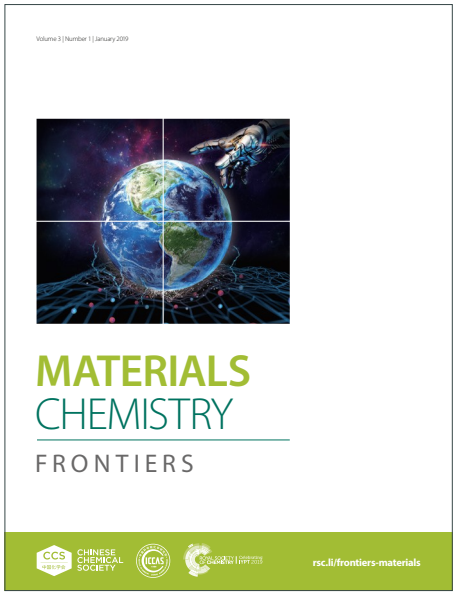

View Article Online
DOI: 10.1039/D6QM00261G

Accessible Electrodeposition of Vinyl-Based Polymer Networks for Tunable and Permselective Ultrathin Coatings

Authors

Colin J. Howard,[1†] Jin Yan,[1†] Amira Oladokun,[2†] Zhaoyi Zheng,[1] Brendon Jaeger,[1] Wenlu Wang,[1] Jörg G. Werner[1,2,3]*

Affiliations

[1] Division of Materials Science and Engineering, Boston University, Boston MA, USA
[2] Department of Chemistry, Boston University, Boston MA, USA
[3] Department of Mechanical Engineering, Boston University, Boston MA, USA
† Contributed equally
* Corresponding author, email: jgwerner@bu.edu

View Article Online
DOI: 10.1039/D6QM00261G

ABSTRACT

Electrodeposition of polymer networks (EPoN) has emerged as an effective method for forming conformal ultrathin polymer coatings through surface-confined electrochemically activated crosslinking under mild solution conditions. Here, we introduce a facile copolymer-based EPoN design in which a small fraction of comonomer units carries phenolic electrochemical crosslinkers, while the majority monomer composition defines the film properties. This design expands the range of polymer chemistries for EPoN to most vinyl-based polymers accessible by radical polymerization and avoids reliance on advanced synthetic equipment or knowledge. To demonstrate this broadly accessible fabrication concept, poly(methyl methacrylate) is obtained from free radical polymerization with a small fraction of glycidyl methacrylate co-monomer that is functionalized with phenolic side groups in a simple one-step procedure. This accessible design enables the electrodeposition of polymers as ultrathin and conformal network coatings on planar and porous conductive substrates with uniform thickness below 200 nm. We demonstrate that both thickness and small-molecule permeability of the polymer network coating are tunable by the phenol fraction in polymer, the deposition potential, and the polymer concentration, while the thin films are impermeable to macromolecules. This work advances EPoN as a versatile and accessible platform for ultrathin polymer coatings by decoupling deposition from film chemistry, thereby enabling broad compositional flexibility and application spaces.

View Article Online
DOI: 10.1039/D6QM00261G

1. Introduction

Ultrathin coatings are surface-confined layers that regulate interfacial transport and surface properties across diverse material systems, with applications in energy conversion and storage,[1-4] optoelectronics,[5,6] sensing devices,[7-9] antimicrobial surface protection,[10] and separation such as carbon capture.[11,12] Desired properties of such coatings include electronic insulation, mechanical and chemical protection, as well as permselectivity. Crosslinked polymer networks conceptually achieve these coating needs as tunable and multifunctional materials combining chemically versatile monomer functionality with tunable network architecture and physical robustness due to their insolubility. In many of these applications, three-dimensional (3D) and porous substrates are especially attractive because their high surface area and tunable architectures can enhance mass and energy transfer,[13] reactivity, and overall device performance.[14] However, fabricating uniform ultrathin (<100 nm) polymer coatings on planar or 3D substrates comes with challenges such as dewetting, or shadowing in line-of-sight depositions and pooling, respectively.[15] These limitations are particularly severe within porous substrates with complex pore geometries or high pore aspect ratios.

Existing strategies to fabricate ultrathin polymer coatings on porous and non-planar substrates include both vapor-phase and solution-based methods. Initiated and oxidative CVD (i/o-CVD) allow vapor-phase deposition of polymer thin films,[16,17] but their continuous growth makes film uniformity increasingly sensitive to reactant transport and local accessibility in high-aspect-ratio, recessed, or diffusion-limited porous structures. Plasma polymerization enables adherent coatings on complex substrates but is highly process-sensitive and limited by precursor volatility in low-pressure implementations.[18] Molecular layer deposition (MLD) provides strong thickness control and 3D conformality through self-limiting vapor-phase growth, at the cost of requiring vacuum processing and compatible volatile monomers.[19] By comparison, layer-by-layer (LbL) deposition is a simple and solution-based method for constructing polymer thin films, offering nanoscale control over film thickness and strong topographic conformity on complex and porous substrates. However, because its assembly mechanism typically relies on electrostatic or other strong complementary interactions, it is generally restricted to charged or highly polar polymers, limiting its compatibility with many low-polarity and hydrophobic polymer systems.[20]

To overcome the above challenges for polymer-network coatings on porous materials, a deposition strategy is required that follows self-limiting or decelerating thin-film growth while also decoupling polymer identity from deposition mechanism. To achieve this for conductive substrates, we previously introduced the electrodeposition of polymer networks (EPoN), a broadly applicable, vacuum-free method carried out under mild solution conditions that produces conformal, uniform, and defect-free ultrathin functional coatings on planar, non-planar, and porous conductive substrates alike.[21-23] Briefly, EPoN utilizes a small fraction of electrochemically activated crosslinkers (eX-linkers) appended to pre-synthesized polymers of interest to enable their electrodeposition as networks. The electrochemically mediated polymer crosslinking confines the network growth to the electrode surface, while the electronic insulation and the macromolecular

View Article Online
DOI: 10.1039/D6QM00261G

impermeability of the growing polymer network results in self-limiting thin-film growth. For example, prior EPoN iterations utilized phenolic eX-linkers attached to telechelic homopolymers as end-groups or to reactive homopolymers as side groups in small fractions.[21,23] We emphasize that EPoN as an electroplating process is limited to fabricate coatings on conductive materials, which are common in energy storage/conversion, sensing, or microelectronics, as well as in corrosion protection of metals, and even in purification and separation applications that are often based on sorption using porous carbon materials with high surface area, which are conductive and applicable to be coated with thin polymer films using our EPoN method.

To broaden the scope of EPoN and increase its accessibility, here we introduce a generalizable synthesis and deposition framework using a random-copolymer design from facile free radical polymerization (FRP) and one-step modification that is compatible with a wide range of vinyl-based polymers. Specifically, a minority comonomer provides a handle for the installation of phenolic eX-linkers, while the majority monomer composition determines the properties of the deposited film. We demonstrate that this architecture preserves the quickly decelerating, surface-confined growth behavior of EPoN while rendering specialized synthetic equipment unnecessary, increasing the applicability of EPoN. We further establish how copolymer composition and deposition conditions govern film formation, thickness, uniformity, and molecular permeability, thereby advancing EPoN toward a general and more tunable route to ultrathin (co)polymer network coatings on planar and porous conductive substrates alike.

2. Experimental

Random copolymers of poly(methyl methacrylate-co-glycidyl methacrylate) [P(MMA-GMA)] with target monomer fractions are synthesized using a thermally initiated free-radical polymerization (FRP) procedure. Following synthesis, phenolic eX-linkers are attached to all GMA co-monomer units via base-catalyzed thiol-epoxy addition using 4-mercaptophenol. Monomer fractions and successful phenol attachment are verified using proton Nuclear Magnetic Resonance (^{1}H NMR). All electrodepositions are performed with potentiostats in custom three-electrode electrodeposition cells where a conductive substrate serves as the working electrode whose active area is confined to a circle of 15 mm diameter with an O-ring, a platinum-wire serves as the counter electrode, and with a silver-based reference electrode. Depositions are performed with either cyclic voltammetry (CV) or potentiostatic with chronoamperometry (CA) under various conditions described in the text. Permeability testing of the deposited coatings is performed by comparing CV scans of a mixed solution of decamethylferrocene (DmFc) and 3.4 kg mol^{-1} poly(ethylene oxide)-diferrocene (PEO-2Fc) before and after EPoN was performed. Unless otherwise specified, all potentials are reported versus the half-wave potential of the DmFc redox probe measured right before each deposition. 3D porous carbon substrates are fabricated via a non-solvent induced phase inversion (NIPS) process reported previously.[23] For deposition on the porous carbon substrate the same three electrode cell is used, with the carbon substrate adhered to a stainless-steel disc as the working electrode and a pulsed potentiostatic deposition procedure. The thickness of all planar films is reported as an average of independent interferometry

View Article Online
DOI: 10.1039/D6QM00261G

measurements taken at three to five discrete and randomly selected locations across the film surface (Table S3). Polymer coatings on the 3D porous carbon substrates are analyzed using scanning electron microscopy (SEM) and thickness is measured using the ImageJ image analysis software at various locations. Detailed experimental procedures are provided in the supporting information.

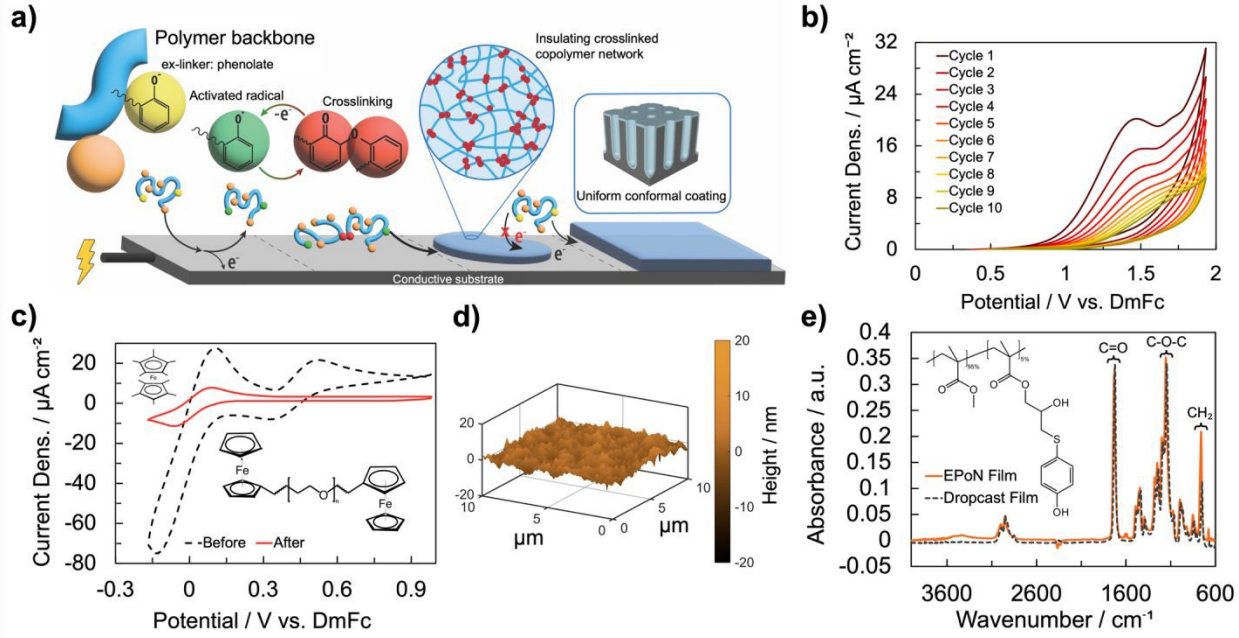

Figure 1. *(a) Schematic of proposed self-limiting growth mechanism for the electrodeposition of polymer networks (EPoN) of (co)polymers: phenolate as crosslinker side groups (yellow) are electrochemically activated by oxidation at the conductive surface of the substrate, generating radicals (green) which couple into crosslinks (red) to form a polymer network near the surface. The orange units represent the majority side group of choice (here: methyl methacrylate or "MMA") of the copolymer that defines its properties and function. (b) Cyclic voltammetry (CV) of a PMMA-5%Ph on an ITO-coated glass substrate, demonstrating passivation of the electrode surface as an insulating film is deposited. (c) CV scans of a solution containing decamethylferrocene (DmFc. left peaks) and 3.4 kg mol^{-1} poly(ethylene oxide)-diferrocene (right peaks) before (black) and after (red) CV deposition of PMMA-5%Ph, demonstrating the permeability of the small DmFc molecule and lack of access to the large polymeric probe after EPoN, indicating complete coverage. (d) AFM height profile on the surface of the EPoN-derived PMMA-5%Ph film on ITO-coated glass shown in (b). (e) ATR-FTIR spectrum for PMMA-5%Ph film deposited on gold using EPoN (solid line) compared to a control spectrum of drop-cast PMMA-5%Ph (dashed line). (b,c) Potential axes are referenced to the half-wave potential of DmFc.*

3. Results and Discussion

Design and EPoN of Vinyl-Based Copolymers: Fundamentally, EPoN utilizes a small fraction of eX-linkers to enable the electrochemical formation of crosslinked polymer networks near the surface. The hypothesis behind the successful use of EPoN for uniform and conformal thin-film deposition requires fast crosslinking and precipitation of the electrochemically activated polymers to ensure adhesion of the formed polymer network to the surface causing its progressive passivation. For anodic electrodeposition, phenol has proven itself an effective eX-linker for its ability to quickly couple and oligomerize upon repeated and continued oxidation to form a crosslinked and insulating polymer network coating on the electrode surface (Fig. 1a).[21,23] We

View Article Online
DOI: 10.1039/D6QM00261G

have previously shown that homopolymers with reactive moieties in each monomer can be electrodeposited as conformal thin films after attachment of a few percent phenol to the reactive backbone.[23] To make more polymers accessible to EPoN, we introduce a new copolymer design that does not rely on reactive homopolymers: a large fraction of the desired monomer(s) defines the thin-film properties, while a small fraction of a reactive co-monomer provides the handle to attach the eX-linker. The use of such random copolymers is a pathway for the simple synthesis and deposition of a wide number of functional polymer films.

Based on this concept, random copolymers of poly(methyl methacrylate-*co*-glycidyl methacrylate) [P(MMA-GMA)] were designed and synthesized. Here, MMA represents the majority monomer making up the copolymer and defining its properties, while GMA is introduced as a minority co-monomers with a reactive epoxy group to which a phenolic eX-linker is appended for EPoN deposition. P(MMA-GMA) copolymers with small GMA monomer fraction (5%, 10%, and 20%) are synthesized and subsequently phenolic eX-linker side-groups are added to all GMA monomers with thiol-epoxy ring-opening addition. Copolymers are named using the monomer fraction percentage, where PMMA-xPh represents a copolymer initially with x GMA monomer fraction that are chemically appended with phenol groups. ^{1}H NMR confirms the copolymer fractions and full conversion of the GMA monomers to phenolic eX-linkers by comparing peak areas of the methoxy group (MMA) to the epoxy region protons (GMA) and their replacement by aromatic protons upon phenol addition (Fig. S1). The molecular weight of the PMMA-5%Ph copolymer was determined by gel permeation chromatography (GPC), yielding a M_n of 97.9 kg mol^{-1} and M_w of 179.8 kg mol^{-1} with a dispersity $Đ$ of 1.84 relative to a polystyrene standard calibration. The size and dispersity are expected for free radical polymerization and well above the entanglement weight for PMMA polymers at around 10 kg mol^{-1} (Table S1).[24]

Deposition and characterization data for a PMMA-5%Ph polymer is shown in Figure 1 as a representative example. Cyclic voltammetry (CV) scans show the phenolic side groups oxidize at a potential above 0.9 V vs. decamethyl ferrocene (DmFc), causing polymer crosslinking and deposition on the electrode surface (Fig. 1b). Successive CV cycles during deposition show progressively lower current density as more cycles are passed. This indicates the conductive surface is being passivated by the deposition of an insulating film, quickly decelerating the growth process to almost self-limiting and defect correcting, leading to uniform and conformal ultrathin films. Comparing this curve to a control CV with unmodified P(MMA-GMA) copolymer demonstrates that the observed current is from the oxidation of the attached phenol groups only (Fig. S2).

To investigate the permeability and coverage of EPoN-derived thin films, CV scans are performed in a solution of DmFc and a poly(ethylene oxide) containing two ferrocene end groups (PEO-2Fc) before and after deposition (Fig. 1c). DmFc is a small molecule that is expected to exhibit permeability through the THF-swollen PMMA network thin-film. Indeed, the oxidation and reduction peak of DmFc are maintained after EPoN of PMMA-5%Ph albeit at lower current density, as is expected from the decreased diffusivity through the crosslinked coating. On the

View Article Online
DOI: 10.1039/D6QM00261G

contrary, the macromolecule PEO-2Fc with a molecular weight of 3.4 kg mol^{-1} is expected to have substantially lower permeability through the PMMA network and, thus, serves as an indirect electrochemical probe for the achieved coverage of the surfaces. The complete absence of its oxidation current above 0.35 V and reduction current above 0.12 V vs. DmFc on the reverse scan reveals that molecules of size similar or larger than 3.4 kg mol^{-1} PEO are unable to reach the conductive surface. This result further proves the complete coverage of the substrate by the EPoN-derived thin film within the electrochemical detection limit.

EPoN-derived ultrathin polymer network films are shown to be conformal and uniform on planar substrates, even below 100 nm: on the macroscale, the average film thickness of the CV EPoN-derived PMMA-5%Ph film on ITO-coated glass, shown in Figure 1b, is 86 nm with a standard deviation of 0.6 nm, determined from three randomly selected spots across the circular area of 15 mm in diameter. On the microscale, atomic force microscopy (AFM) height profiling across the film surface shows the smoothness of the thin film with a roughness (R_a) of 1.2 nm and height deviations within +/- 5 nm over the 10 µm by 10 µm scanning area (Fig. 1d). To confirm that the polymer structure is chemically unaltered by the EPoN process and it is, in fact, PMMA that is deposited as a thin film, attenuated total reflectance Fourier-transform infrared (ATR-FTIR) absorption spectroscopy is performed for a film deposited on a gold substrate (Fig. 1e). The obtained spectra are almost identical between the EPoN-derived thin film and a drop-cast control sample. The broad absorption band at 3300–3500 cm^{-1} can be attributed to the hydroxyl stretching vibrations of the phenolic side groups and the ring-opened epoxides.

Film Growth Behavior: To further explore the deposition behavior of the EPoN mechanism, electrochemical-quartz crystal microbalance with dissipation (E-QCM-D) is used for in-situ monitoring of the film growth during EPoN of PMMA-5%Ph at 1.09 V vs. AgQRE on a gold coated quartz crystal substrate. Upon applying the oxidative potential, a fast drop in resonant frequency together with an increase in dissipation is observed, indicating the deposition of a non-rigid or viscoelastic film on the electrode surface (Fig. 2a). The transient change in QCM-sensor response is used to model the thickness of the depositing film over time (Fig. 2b). During the early stage of deposition, the current density decreases rapidly while the film thickness increases quickly, suggesting rapid passivation and film growth. The modelled film thickness continues to increase throughout the 1200-s deposition at a rate lower than the initial growth, consistent with the growth of an insulating polymer network that densifies on the electrode surface and reduces macromer transport but seemingly inconsistent with a fully self-limiting growth mechanism. It is interesting to observe that the current density drops off at a much sharper rate than the film thickness grows in the E-QCM-D.

The modeled thickness trace also exhibits an intermediate change in growth rate at longer deposition times, corresponding to a temporary plateau-like feature in the QCM frequency and dissipation response followed by a quick increase of the dissipation response and splitting between the overtones. This behavior could reflect changes in solvent uptake and mechanical response of the crosslinked polymer network at this point (>400 s) during deposition, rather than a transition

View Article Online
DOI: 10.1039/D6QM00261G

to increased growth kinetics. The dry-film thickness measured on the same film after the 1200-s E-QCM-D deposition is 71 nm, while the final thickness from the viscoelastic model fitted to the QCM-D response yields is around 200 nm. This difference could be attributed to solvent swelling of the crosslinked polymer network during the in-situ QCM-D measurement in THF, together with uncertainty associated with viscoelastic modeling of soft polymer films (swelling vs. growth).

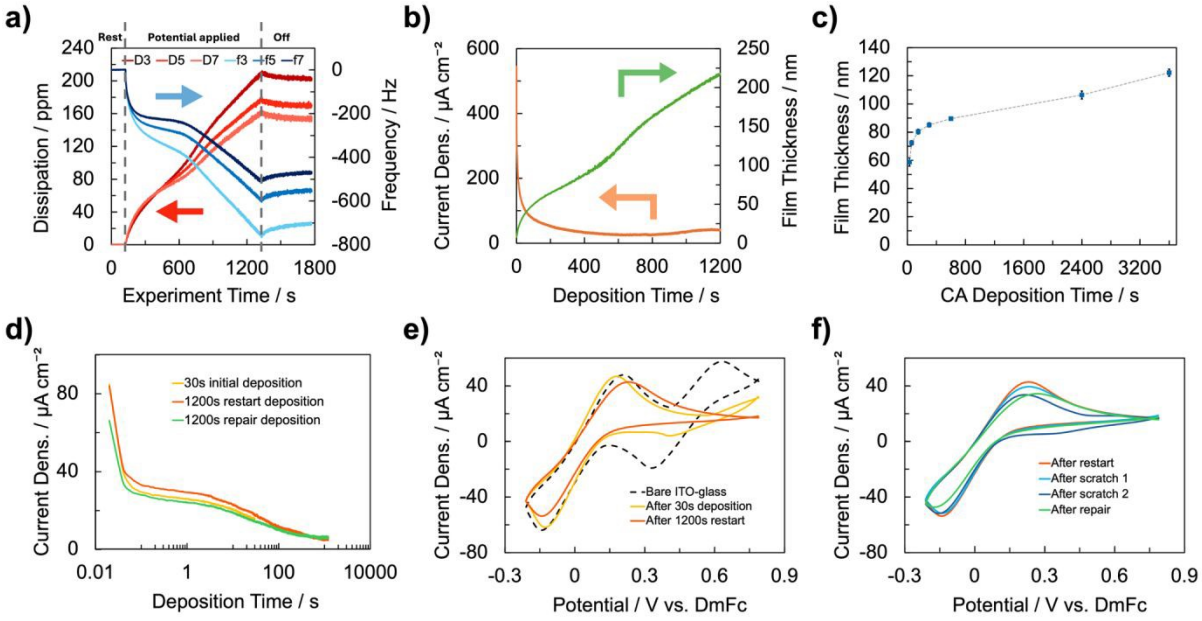

Figure 2. *(a) E-QCM-D response data for three overtones (n = 3,5,7) during the in-situ growth study of PMMA-5%Ph at 1.09 V vs. AgQRE on a gold-coated quartz-crystal sensor. (b) Current density and modelled in-situ film thickness from the E-QCM-D deposition of PMMA-5%Ph at 1.09 V vs. AgQRE. (c) Ex-situ dry film thickness obtained from interferometry for potentiostatic depositions of PMMA-5%Ph on ITO-coated glass at 1.09 V vs. AgQRE after different EPoN times from 30 to 3600 seconds. (d) Current density for potentiostatic depositions at 1.09 V vs. AgQRE on an ITO-coated glass substrate during the restart and repair experiments of PMMA-5%Ph, with initial 30-second deposition (yellow), the 1200-second restarted deposition (orange), and 1200-second repair deposition after damage (green). (e) CV scans of a mixed-ferrocene solution containing decamethylferrocene (redox peaks < 0.3 V vs. DmFc) and 3.4 kg mol^{-1} poly(ethylene oxide)-diferrocene (redox peaks > 0.3 V vs. DmFc) before any deposition (black dashed), after the initial deposition (yellow), and after the restarted deposition (orange). (f) CV scans of the PMMA-5%Ph coated ITO substrate from (d) in the same mixed-ferrocene solution as in (e) after the restarted deposition (orange) compared to after the first needle scratch (light blue), second scratch (dark blue), and after the repair deposition (green).*

To further quantify the transient film growth, a complementary ex-situ growth study is conducted by measuring the dry-film thickness of PMMA-5%Ph coatings deposited at 1.09 V vs. AgQRE (≈ 1.3 V vs. DmFc) on ITO coated glass for varying deposition times from 30 to 3600 seconds (Fig. 2c). For all seven depositions, a substantial current drop is observed over the first 100 s, further demonstrating the rapid electrochemical passivation rate (Fig. S3). Based on the dry-film thickness after each distinct deposition time, the films exhibit a rapid initial growth, with over two thirds of the final thickness accumulated in the first ~300 s of deposition, followed by substantially slower continued growth at longer deposition times. These ex-situ results confirm a distinct slow-down of the film growth beyond 300 s, but the slow continued growth renders EPoN of this polymer not fully self-limiting. The apparent differences observed between the transient in-

View Article Online
DOI: 10.1039/D6QM00261G

situ E-QCM-D and ex-situ film thickness may stem from the difference in deposition cell geometry, working electrode (gold vs. ITO), and modelling of the viscoelastic thin film.

To further investigate the transient growth behavior of EPoN, a potentiostatic deposition is performed with PMMA-5%Ph (140 mg mL^{-1}) for only 30 seconds at 1.09 V vs. AgQRE (≈ 1.3 V vs. DmFc), followed by film drying and characterization before continuing the deposition for 1200 seconds under the same conditions. The current response following the restarted deposition exhibits a transient response similar to the initial 30-s deposition process (Fig. 2d), indicating continued electrochemical growth after drying and rewetting of the polymer-coated substrate. The DmFc/PEO-2Fc permeability CV test further confirms transient evolution of film transport properties during early stages of EPoN (Fig. 2e): after the initial 30-s deposition, the smaller DmFc probe largely retains its accessibility to the electrode surface, while the macromolecular PEO-2Fc signal is partially suppressed, indicating formation of a film with finite but diminished macromolecular permeability. The measured dry-film thickness after the 30-s deposition is 35 nm (Table S2). Following the second 1200-s deposition under identical conditions, the PEO-2Fc signal is completely suppressed and the dry-film thickness reaches 81 nm, consistent with measured 90 nm for a single 1200-s deposition. These results demonstrate that EPoN growth can be interrupted prematurely and restarted for continued film growth even after drying of the film, leading to similar outcomes as a non-interrupted deposition.

Since EPoN deposits polymer networks as thin films on all solution-accessible conductive surfaces, it is feasible to repair damaged coatings. To this end, two types of localized damage are introduced to an EPoN-derived PMMA-5%Ph film (1.09 V vs. AgQRE ≈ 1.3 V vs. DmFc, 140 mg mL^{-1}). First, a sharp needle is used to generate several small scratches accumulating to roughly 1.3% of the film area, which produces negligible changes in CV-measurable film permeability (Fig. 2f and S4). Second, a THF-wetted cotton swab is used to generate a larger damaged region (10% of film area), resulting in the emergence of a small PEO-2Fc signal during the CV permeability test, consistent with the fraction of exposed ITO substrate. The damaged film is subsequently repaired with EPoN of an additional 1200 s under identical conditions of its initial deposition. After repair, the region of the needle damage (scratch 1) regrows to a thickness of 89 nm (Table S2), matching the expected thickness for a fresh 1200-s deposition under the same conditions. The larger damaged region (scratch 2) exhibited a slightly higher thickness of 112 nm after repair, possibly due to changes in surface activity of the damaged ITO substrate. Overall, this experiment demonstrates that EPoN is defect-correcting and can be used for repair of damaged thin-film coatings.

Effects of Deposition Conditions: With the goal of identifying composition-processing-property relationships that can be used as knobs to tune the properties of the EPoN-derived polymer thin films, we study the impact of phenol percentage (x=5%, 10%, 20%), deposition potential, and addition of tripropylamine (TPA) as a base to deprotonate the phenol eX-linker.. The three deposition potentials are chosen to represent the three types of electrochemical regimes in the absence of TPA (Fig. 1b): 0.9 V vs. DmFc for the onset of phenol oxidation (charge-transfer

View Article Online
DOI: 10.1039/D6QM00261G

kinetics dominate), 1.7 V vs. DmFc well beyond the phenol oxidation peak (mass transfer dominates), and 1.3 V vs. DmFc as a mixed regime between those two extremes. As expected, the initial current is universally higher for higher deposition potentials. However, depositions without base passivate quickly even at the highest potential (Fig. 3a), while higher and continuous current is passed over the whole deposition time of 20 minutes in the presence of the TPA base (Fig. 3b and Fig. S5).

We hypothesized that this high sustained anodic current is contributed by the electrochemical oxidation of TPA under the applied deposition conditions. Control experiments consisting of only TPA in supporting electrolyte (0.5 M TBAP in THF) show an oxidation onset potential of TPA at around 1 V vs. DmFc and a current decay after 6 repeated CV cycles, indicating that TPA is oxidized and may contribute to transient interfacial changes or surface passivation (Fig. S6b). Potentiostatic oxidation of TPA at 1.09 V vs. AgQRE (≈ 1.3 V vs. DmFc) also exhibits sustained anodic current under (Fig. S6d). However, despite its irreversible electrochemical oxidation, no measurable film formation is observed in the absence of our PMMA-xPh polymers, and electrochemical permeability tests confirm that both small-molecule and macromolecular probes retain full accessibility to the substrate following TPA oxidation (Fig. S6c,e). These results demonstrate that TPA itself does not independently generate a crosslinked insulating or passivating coating. Therefore, the sustained current observed in TPA-containing depositions likely reflects contributions initially from both the oxidative polymer deposition and the TPA oxidation, and is later dominated by TPA oxidation since the deposited PMMA-xPh films are permeable to such small molecules. Thus, the deposition current alone cannot be directly interpreted as an indicator of film growth or surface passivation if another electrochemically active small molecule is present.

Deposition at the lowest potential where charge transfer kinetics dominate result in uniform thin films with thicknesses ranging from 37-87 nm depending on phenol fraction and presence of the TPA base (Fig. 3c and Table S3). The film thickness increases under all conditions for the intermediate deposition potential, with a maximum of around 130 nm for deposition of PMMA-5%Ph with TPA present. Interestingly, the film obtained at the highest EPoN potential without TPA catalyst is substantially thinner (73 nm) compared to the intermediate potential case, while the TPA-containing conditions appear to reach a steady thickness at higher potentials. We postulate that the presence of the TPA base alters the electrochemical environment during deposition, resulting in similar outcomes for both 1.3 and 1.7 V vs. DmFc, while a significant change of the growth is observed over this potential range without TPA. Similarly, higher phenol fractions also led to thinner films at the intermediate and high deposition potential, likely due to faster network densification (crosslinking) and passivation of the electrode, limiting further polymer access to the surface for phenol oxidation (Fig. S6f). Comparing PMMA-5%Ph with and without base catalyst, despite a more than 5 times higher current during deposition in the presence of TPA, it only shows a small increase in the resulting film thickness (Fig. 3c). We do note, however, that the precise effect of TPA oxidation on the crosslinking chemistry, as well as any possible side reactions with the phenol or copolymer, remains unclear at this stage.

View Article Online
DOI: 10.1039/D6QM00261G

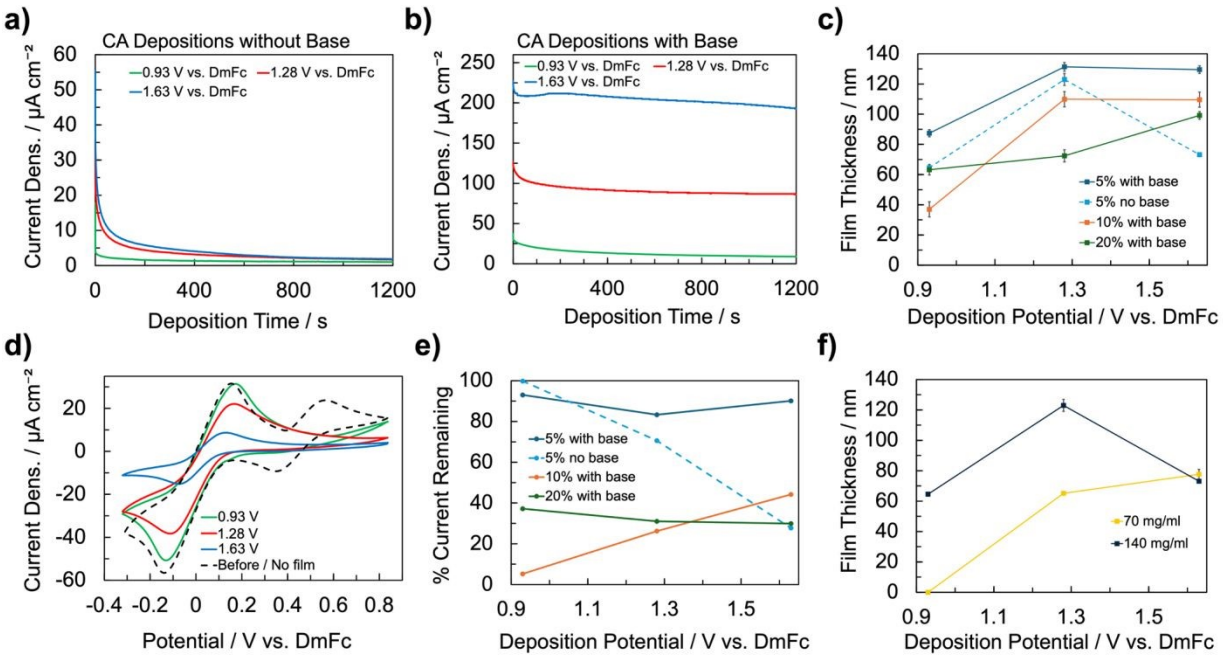

Figure 3. *(a-b) Chronoamperometry (CA) of the constant potential depositions of PMMA-5%Ph at three different potentials without (a) and with tripropylamine (TPA) as a catalytic base (b). (c) Film thickness of the potentiostatic EPoN-derived PMMA-xPh films deposited at three different potentials with x = 5%, 10%, and 20%, with and without TPA base for x = 5%. (d) Cyclic voltammetry scans in solution of decamethylferrocene (left redox peaks) and 3.4 kDa poly(ethylene oxide)-diferrocene (right redox peaks) overlayed for PMMA-5%Ph films deposited with no base at three different potentials compared to bare ITO coated glass (dashed). (e) Relative peak oxidation current of decamethylferrocene remaining after EPoN of for PMMA-xPh films with x = 5%, 10%, and 20% deposited at three different potentials with and without base for x = 5% on ITO coated glass. More remaining current indicates higher film permeability to small molecules. (f) Film thickness of PMMA-5%Ph deposited on ITO coated glass at three different potentials and two polymer concentrations. (c,f) Values and error bars plotted represent the mean and standard deviation, respectively, of interferometric thickness measurements in at least three distinct random locations.*

Importantly, all tested EPoN conditions yielded thin films that are homogeneous in thickness and fully covering the substrate, as evidenced by the blocking of the PEO-2Fc from the electrode (Fig. 3d and Fig. S7). The decrease in peak oxidation current of the DmFc after EPoN deposition demonstrates the permeability of the obtained thin films to small molecules, though the magnitude of permeability is not correlated to their thickness. For example, PMMA-5%Ph is thickest when deposited at the intermediate potential, but least permeable from the highest deposition potential (Fig. 3d,e). This result is consistent with the molecular picture that networks with higher crosslink density swell less and are harder for molecules to permeate through. A similar relationship based on crosslink density is observed with a change in phenol% of the copolymer: although films are of similar thickness or even thinner at higher phenol%, these films are less permeable to the small molecule DmFc (Fig. 3e).

Lastly, the polymer solution concentration is an additional impactful process parameter to change the thickness of polymer coatings. Specifically, PMMA-5%Ph depositions at a lower concentration of 70 mg mL^{-1} (half the concentration of all previous depositions discussed) without TPA present yielded measurable film thickness only at the intermediate and high deposition potentials (Fig. 3f and Fig. S8). While the film deposited at the intermediate potential is half the

View Article Online
DOI: 10.1039/D6QM00261G

thickness at 70 mg mL^{-1} compared to 140 mg mL^{-1}, the highest potential resulted in similar film thickness. Additionally, some permeability to the large polymeric probe PEO-2Fc remains at the low polymer concentration, likely due to either a low crosslinking density or possible uncoated areas (Fig. S7). At the lowest potential of 0.9 V vs. DmFc, no consistent continuous thin film is deposited with 70 mg mL^{-1} PMMA-5%Ph, as seen by optical microscopy revealing only a few spotty clumps of polymer precipitated onto the ITO-coated glass substrate (Fig. S9).

Overall, while a strong dependency of films thickness and permeability on some composition-process conditions is observed, the EPoN-derived films are highly uniform with relative standard deviations of less than 10% of the film thickness for all samples measured at random locations over the circular film area of 15 mm diameter, and with 13 of the 15 samples exhibiting relative standard deviations below 5% (Table S3). We postulate this uniformity to be a result of the growth rate that substantially slows down over time resulting in an almost self-limiting growth inherent to the EPoN concept.

EPoN on a Porous 3D Substrate: The biggest struggle of conventional polymer coating techniques is their conformal deposition on 3D structured surfaces or porous substrates. Mass-transport or line-of-sight limitations often lead to non-uniform deposition near pore entrances, preventing uniform coating deeper inside the pores. In previous studies, EPoN was shown to overcome these limitations through its self-limiting and defect-correcting growth mechanism, enabling conformal and uniform ultrathin coatings on porous conductive architectures. Here, we further evaluate the applicability of this mechanism to the present copolymer system. Porous carbon electrodes with through-plane channeled pores on the micron scale that are open on one side are used to test the EPoN of PMMA-5%Ph on a porous 3D substrate. Due to the thickness dependence on polymer concentration, a pulsed potentiostatic deposition is used with a 50 s rest period at open-circuit potential between pulses to allow the polymer concentration to frequently equilibrate throughout the deposition (Fig. 4a). Two depositions, one with longer 10-seconds and one with shorter 1-second pulses, are performed. For both, the current decreases quickly over first 10 pulses implying the deposition of a passivating film, while the appearance of a steady state suggests that the majority of the polymer is deposited within the first fifty cycles, even for a short pulse duration of 0.1 second (Fig. S10). Mixed ferrocene characterization before and after shows the coating is still permeable to polymeric and small-molecule ferrocene probe, providing an inconclusive result with regards to film coverage and conformality (Fig. S11). However, SEM cross-sectional images before and after deposition provide evidence for the presence and conformality of the film (Fig. 4b). High-resolution SEM image before EPoN (10-second pulses) show the porous carbon substrate with a dense surface topography of the micron-sized channel pores with diameters around 5-10 μm and nanoporosity within the wall between them. Cross-sectional SEM images after EPoN show conformal PMMA film coating throughout the micron-sized channel pores. Using image analysis measurements, the polymer coating is relatively uniform with thicknesses in the range of 116-170 nm at the tops, middles and bottoms of pores (Fig. S12 and Table S4).

View Article Online
DOI: 10.1039/D6QM00261G

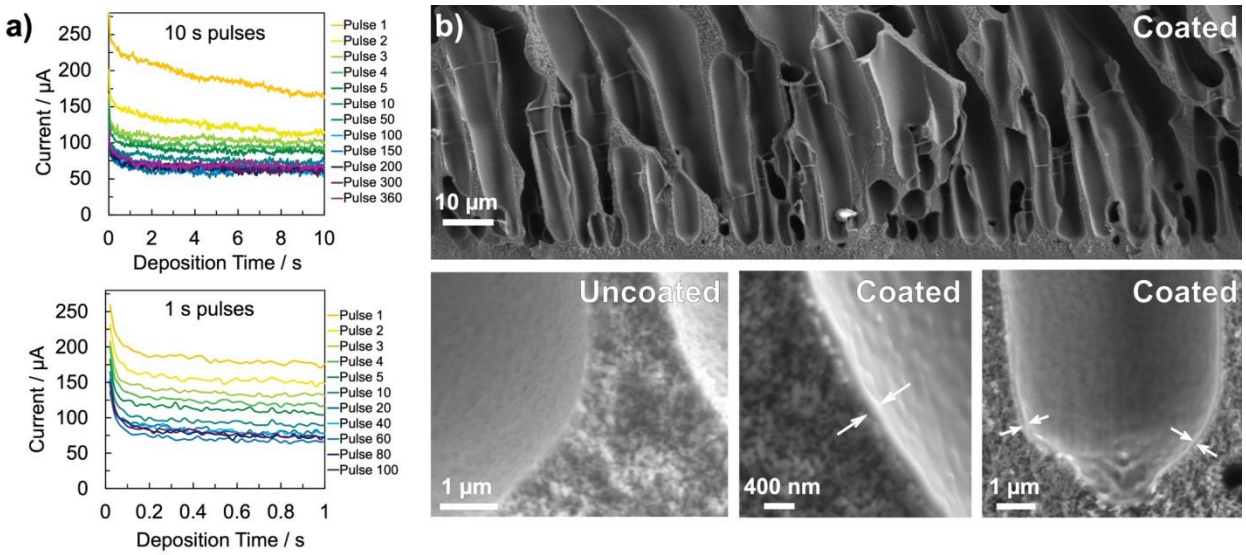

Figure 4. *(a) Chronoamperometry of select potentiostatic pulses during electrodeposition of PMMA-5%Ph on porous 3D carbon substrates at 1.09 V vs AgQRE with 10 s pulses (top) and 1s pulses (bottom), both featuring a 50s rest period between pulses. (b) SEM images showing the entire cross-section of the porous 3D carbon substrate (top) and the pore surface before (bottom left) and after EPoN of PMMA-5%Ph with 10-second pulses at the middle of a cylindrical pore (bottom middle) and bottom of a cylindrical pore (bottom right). The deposited film is indicated by white arrows. Additional SEM images and thickness measurements provided in the Supporting Information.*

4. Conclusion

EPoN is an effective strategy for the conformal deposition of uniform ultrathin coatings of polymer networks on planar and porous conductive substrates alike. In this work, we extend the scope of EPoN to a broader range of (co)polymers through a macromolecular design that introduces a minor fraction of reactive comonomer as the attachment point for phenolic eX-linkers to the majority monomer(s) that defines the film properties, all accessible through facile free-radical polymerization and one-step modification. With phenol-functionalized P(MMA-GMA) as an example, we show that its EPoN exhibits surface-passivating and quickly decelerating growth behavior that enables conformal ultrathin polymer coatings on both planar and 3D conductive substrates. While the composition-processing-property relationships are non-linear and even non-monotonic, we established guidelines for tuning EPoN-derived ultra-thin coatings: Film thickness and permeability can be tuned through deposition potential, polymer concentration, and phenol percentage. Higher polymer concentrations and potentials well beyond phenol oxidation favor faster network densification and yield thin, dense, low-permeability coatings, whereas lower concentrations or potentials closer to the oxidation onset produce thinner, more permeable films. Thicker films with high permeability are favored at lower phenol fraction and at intermediate potentials, where slower densification allows more prolonged film growth. In addition, pulsed-potential deposition demonstrates that EPoN can provide uniform coatings on complex 3D porous architectures. More broadly, this work highlights the versatility of EPoN as a general platform for ultrathin polymer coatings, with the flexibility to accommodate diverse

View Article Online
DOI: 10.1039/D6QM00261G

polymer compositions and film chemistries. By separating the eX-linkers from the majority composition, this copolymer platform enables independent control over film formation, topography, and chemistry. We envision this synthetically simple and highly tunable process to enable researchers and industry to fabricate tailored interphases and interfacial properties for surface protection, controlled wettability, molecular separation and purification such as carbon capture, as well as energy storage and conversion.

Author contributions

All authors have given approval to the final version of the manuscript. JGW devised the original idea and supervised the research project. AO, JY and CH conducted the copolymer synthesis, electrodeposition, characterization of the films and data analysis. BJ fabricated the 3D carbon electrodes. WW instructed the electrodeposition on 3D carbon electrodes and assisted with SEM imaging. ZZ assisted with the interferometry measurements and E-QCM-D measurements. JGW, JY and CH wrote the manuscript for publication.

Data availability

The data supporting this article have been included in the Electronic Supporting Information (ESI).

Conflicts of interest

The authors declare that they have no known competing financial interests or personal relationships that could have appeared to influence the work reported in this paper.

Acknowledgements

The research was in part sponsored by the Army Research Office and was accomplished under Cooperative Agreement Number W911NF-25-2-0074. The views and conclusions contained in this document are those of the authors and should not be interpreted as representing the official policies, either expressed or implied, of the Army Research Office or the U.S. Government. This work was performed in part at the Harvard University Center for Nanoscale Systems (CNS); a member of the National Nanotechnology Coordinated Infrastructure Network (NNCI), which is supported by the National Science Foundation under NSF award no. ECCS-2025158. WW and JGW acknowledge support for this work from the National Science Foundation under Grant No. CBET-2146597. The authors thank Gunho Lee for assisting with the FT-IR measurements. The authors thank Prof. Mark Grinstaff and his group at Boston University for providing access to the GPC instrument, and Madeline K. Loffredo for performing the GPC measurements.

View Article Online
DOI: 10.1039/D6QM00261G

References

1. Y. He, H. Pham, X. Liang and J. Park, Impact of Ultrathin Coating Layer on Lithium-Ion Intercalation into Particles for Lithium-Ion Batteries, *Chem. Eng. J.*, 2022, **440**, 135565.
2. I. D. Scott, Y. S. Jung, A. S. Cavanagh, Y. Yan, A. C. Dillon, S. M. George and S.-H. Lee, Ultrathin Coatings on Nano-$LiCo_2$ for Li-Ion Vehicular Applications, *Nano Lett.*, 2011, **11**(2), 414-418.
3. C. Zhou, Z. Xi, D. J. Stacchiola and M. Liu, Application of Ultrathin TiO_2 Layers in Solar Energy Conversion Devices, *Energy Sci. Eng.*, 2022, **10**(5), 1614-1629.
4. M. Abbasi, Y. Dong, J. Meng, D. Morgan, X. Wang and J. Hwang, *In Situ* Observation of Medium Range Ordering and Crystallization of Amorphous TiO_2 Ultrathin Films Grown by Atomic Layer Deposition, *APL Mater.*, 2023, **11**(1), 011102.
5. T. Wu, L. Tan, Y. Feng, L. Zheng, Y. Li, S. Sun, S. Liu, J. Cao and Z. Yu, Toward Ultrathin: Advances in Solution-Processed Organic Semiconductor Transistors, *ACS Appl. Mater. Interfaces*, 2024, **16**(45), 61530-61550.
6. C. Ding, J. Deng, M. Cheng, M. Li and L. Li, Structural Control of Charge Transport in Polymer Monolayer Transistors by a Thermodynamically Assisted Dip-Coating Strategy, *J. Mater. Chem. C*, 2023, **11**(18), 6026-6033.
7. M. Poonia and A. Singh, Carbon Nanomaterials as Smart Interfaces in Ultrathin Films for High-Performance Electrochemical Sensors: A Critical Review, *RSC Adv.*, 2025, **15**(35), 28897-28917.
8. A. Kumar, S. J. Shivaraja, V. Manjuladevi and R. K. Gupta, Ultrathin Langmuir-Blodgett Film of Functionalized Single-Walled Carbon Nanotubes for Enhanced Acetone Sensing, *Microchem. J.*, 2024, **200**, 110219.
9. C. A. Zattim Jr., H. S. Kavazoi, C. M. Miyazaki and P. Alessio, Investigating Layer-by-Layer Films of Carbon Nanotubes and Nickel Phthalocyanine towards Diquat Detection, *Sci. Rep.*, 2024, **14**, 16582.
10. K. Kamnev, M. Bendova, Z. Fohlerova, T. Fialova, O. Martyniuk, J. Prasek, K. Cihalova and A. Mozalev, Arrays of Ultra-Thin Selenium-Doped Zirconium-Anodic-Oxide Nanorods as Potential Antibacterial Coatings, *Mater. Chem. Front.*, 2025, **9**, 866-883.
11. F. Pazianalenjareghi, S. Singh, F. Attia, V. S. R. Munnangi, E. M. Nsengiyumva, Y. Jiao and H. Lin, Engineering MOFs for Thin-Film and Nanofilm Nanocomposite Membranes for CO_2 Separation, *J. Mater. Chem. A*, 2026, **14**, 4323-4343.
12. S. Fan, C. Liang, F. Feng, K. Wong, K. Wang, S. Jia, N. Bhuwania, S. Zhang and S. Zhang, Polymer-MOF Network Enabling Ultrathin Coating for Post-Combustion Carbon Capture, *Angew. Chem. Int. Ed.*, 2025, **64**, e202421028.
13. X. Zhang, L. Shu, Z. Yang, L. Liu, F. Zhu, H. Wang, Y.-Y.-S. Cheng, Y. Huang and J.-F. Li, Ultra-Thin Multilayer Films for Enhanced Energy Storage Performance, *Nano Energy*, 2024, **121**, 109271.

View Article Online
DOI: 10.1039/D6QM00261G

14. Karimzadeh, B. Safaei, C. Yuan and T.-C. Jen, Emerging Atomic Layer Deposition for the Development of High-Performance Lithium-Ion Batteries, *Electrochem. Energy Rev.*, 2023, **6**(1), 24.
15. R. B. Bird, W. E. Steward, and E. N. Lightfoot, Chapter 17: Diffusion and the Mechanisms of Mass Transport, *Transport Phenomena*, 2nd ed., Wiley, 2002.
16. W. E. Tenhaeff and K. K. Gleason, Initiated and Oxidative Chemical Vapor Deposition of Polymeric Thin Films: iCVD and oCVD, *Adv. Funct. Mater.*, 2008, **18**, 979-992.
17. A. Dianatdar and R. K. Bose, Oxidative Chemical Vapor Deposition for Synthesis and Processing of Conjugated Polymers: A Critical Review, *J. Mater. Chem. C*, 2023, **11**, 11776-11802.
18. B. R. Coad, P. Favia, K. Vasilev and H. J. Griesser, Plasma Polymerization for Biomedical Applications: A Review, *Plasma Process. Polym.*, 2022, **19**, e2200121.
19. H. Zhou and S. F. Bent, Molecular Layer Deposition of Functional Thin Films for Advanced Lithographic Patterning, *ACS Appl. Mater. Interfaces*, 2011, **3**, 505-511.
20. J. Borges, L. C. Rodrigues, R. L. Reis and J. F. Mano, Layer-by-Layer Assembly of Light-Responsive Polymeric Multilayer Systems, *Adv. Funct. Mater.*, 2014, **24**, 5624-5648.
21. W. Wang, A. B. Resing, K. A. Brown and J. G. Werner, Electrodeposition of Polymer Networks as Conformal and Uniform Ultrathin Coatings, *Adv. Mater.*, 2024, **36**, 2409826.
22. Z. Zheng, A. B. Resing, W. Wang and J. G. Werner, Cathodic Electrodeposition of Polymer Networks as Ultrathin Films on 3-D Micro-Architected Electrodes, *RSC Appl. Polym.*, 2024, **2**, 1139-1146.
23. W. Wang, Y. Li, A. B. Resing, J. Yan, Z. Zheng and J. G. Werner, Electrodeposition of Reactive Polymer Networks for Conformal Ultrathin Coatings Amenable to Post-Deposition Functionalization, *J. Mater. Chem. A*, 2025, **13**, 29050-29059.
24. L. J. Fetters, D. J. Lohse, D. Richter, T. A. Witten and A. Zirkel, Connection between Polymer Molecular Weight, Density, Chain Dimensions, and Melt Viscoelastic Properties, *Macromolecules Rev.*, 1994, **27**, 4639-4647.

View Article Online
DOI: 10.1039/D6QM00261G

View Article Online
DOI: 10.1039/D6QM00261G

Data Availability Statement

for

Accessible Electrodeposition of Vinyl-Based Polymer Networks for Tunable and Permselective Ultrathin Coatings

Authors

Colin J. Howard,[1†] Jin Yan,[1†] Amira Oladokun,[2†] Zhaoyi Zheng,[1] Brendon Jaeger,[1] Wenlu Wang,[1] Jörg G. Werner[1,2,3]*

Affiliations

[1] Division of Materials Science and Engineering, Boston University, Boston MA, USA
[2] Department of Chemistry, Boston University, Boston MA, USA
[3] Department of Mechanical Engineering, Boston University, Boston MA, USA
† Contributed equally
* Corresponding author, email: jgwerner@bu.edu

The data supporting this article have been included as part of the Electronic Supplementary Information.